Dalton Transactions

PAPER

View Article Online
View Journal | View Issue

Cite this: *Dalton Trans.*, 2015, **44**, 2871

Preparation, characterization, and properties of PMMA-doped polymer film materials: a study on the effect of terbium ions on luminescence and lifetime enhancement†

Hui-Jie Zhang,[a] Rui-Qing Fan,*[a] Xin-Ming Wang,[a] Ping Wang,[a] Yu-Lei Wang[b] and Yu-Lin Yang*[a]

Received 30th October 2014,
Accepted 9th December 2014

DOI: 10.1039/c4dt03348e

www.rsc.org/dalton

Poly(methylmethacrylate) (PMMA) doped with Tb-based imidazole derivative coordination polymer $\{[Tb_3(\mathbf{L})(\mu_3\text{-}OH)_7]\cdot H_2O\}_n$ (**1**) (**L** = *N*,*N*′-bis(acetoxy)biimidazole) was synthesized and its photophysical properties were studied. The **L′** (**L′** = *N*,*N*′-bis(ethylacetate)biimidazole) ligand was synthesized by an N-alkylation reaction process followed by ester hydrolysis to produce ligand **L**. Polymer **1** and ligand **L′** have been characterized by ^{1}H NMR and IR spectroscopy, elemental analysis, PXRD and X-ray single-crystal diffraction. Coordination polymer **1** is the first observation of a $CdCl_2$ structure constructed with hydroxy groups and decorated by ligand **L** in lanthanide N-heterocyclic coordination polymers. In the 2D layered structure of **1**, each Tb3 metal center is connected with three Tb1 and three Tb2 metal centers by seven hydroxyl groups in different directions, resulting in a six-membered ring. After doping, not only the luminescence intensity and lifetime enhanced, but also their thermal stability was increased in comparison with **1**. When **1** was doped into poly(methylmethacrylate) (**1**@PMMA), polymer film materials were formed with the PMMA polymer matrix (w/w = 2.5%–12.5%) acting as a co-sensitizer for Tb^{3+} ions. The luminescence intensity of the Tb^{3+} emission at 544 nm increases when the content of Tb^{3+} was 10%. The lifetime of **1**@PMMA (914.88 μs) is more than four times longer than that of **1** (196.24 μs). All τ values for the doped polymer systems are higher than coordination polymer **1**, indicating that radiative processes are operative in all the doped polymer films. This is because PMMA coupling with the O–H oscillators from $\{[Tb_3(\mathbf{L})(\mu_3\text{-}OH)_7]\cdot H_2O\}_n$ can suppress multiphonon relaxation. According to the variable-temperature luminescence (VT-luminescence) investigation, **1**@PMMA was confirmed to be a stable green luminescent polymer film material.

Introduction

Luminescent lanthanide materials have received increasing attention for applications in light emitting diodes, luminescence probes, bioimaging, optical electroluminescent and laser materials.[1,2] This is attributed to the fact that the lanthanide–organic frameworks (LnOFs) offer numerous advantages: high photoluminescence efficiency, unique line-like emission bands, substantial Stokes shifts, and long luminescence lifetimes.[3,4] Among the lanthanide ions, Tb^{3+} ion is one of the most important luminescent activators, which is an attractive option for visible luminescent materials owing to its strong green (λ_{em} = 544 nm) emission.[5] However, lanthanide ions present a low molar absorption coefficient for forbidden f–f transitions (Laporte forbidden).[6,7] As a consequence, the direct excitation of the lanthanide ions is unfavorable. To overcome this disadvantage, researchers always introduce π-conjugated organic chromophores to sensitize Ln^{3+} centers through an energy transfer process.[8,9] Among the widely known organic ligands, imidazoline-based and multicarboxylate ligands frequently appear to achieve the requirements for lanthanide luminescence purposes.[10] The imidazole carboxylic acid ligand, in this investigation, has two remarkable features: the N and O atoms in the ligand **L′**, which can coordinate with metal ions to form coordination polymers and $-CH_2-$ group, which can rotate to satisfy the coordination orientation of the carboxylate group to ease steric hindrance.[11] Lanthanide ions

[a]*Department of Chemistry, Harbin Institute of Technology, Harbin 150001, P. R. of China. E-mail: fanruiqing@hit.edu.cn, ylyang@hit.edu.cn; Fax: +86-451-86413710*
[b]*National Key Laboratory of Science and Technology on Tunable Laser, Harbin Institute of Technology, Harbin 150080, P. R. of China*

†Electronic supplementary information (ESI) available: CCDC no. 1015173 contains the supplementary crystallographic data for coordination polymer **1**. CCDC 1015173. For ESI and crystallographic data in CIF or other electronic format see DOI: 10.1039/c4dt03348e

can display various coordination surroundings from VI to XII, forming covalent bonds with oxygen as well as nitrogen in mixed functionalized organic ligands. They can exhibit a diverse range of structures with fascinating topology such as honeycomb, rectangular grid, bilayer lattice, ladder and diamond frameworks.[12,13]

Recently, researchers have been interested in exploring new white/red/green/yellow light emitting materials achieved by doping or changing the excitation wavelength.[14] Inspired by the prominent work of F. Brito, H.J. Zhang, M.L.P. Reddy and other famous chemistry researchers, we consider that lanthanide ions are good candidates for the construction of coordination polymers with excellent luminescent properties.[15–17] To date, lanthanide coordination polymers have the typical shortcomings of relatively low thermal-stability and limited-photoluminescence in their original state.[18] The poly(methylmethacrylate) polymer (PMMA) exhibits excellent mechanical and optical properties that favour its application as the basis for optical devices.[19,20] It is also a low-cost and simply prepared polymer, which has no light absorption longer than 250 nm.[21] Furthermore, the carbonyl groups of PMMA can interact with Ln^{3+} ions and substitute the water molecule ligands. When lanthanide coordination polymers are incorporated into PMMA, they form a new luminescent material possessing excellent thermal stability and photostability.[22–24]

Taking these points into account, we have designed and synthesized a ligand, namely, *N*,*N*′-bis(ethylacetate)biimidazole (**L**′), in which the $-COOC_2H_5$ group can be hydrolyzed into their corresponding carboxylic groups (**L**) using an ester hydrolysis process. To date, transition metal–organic frameworks with ligand **L**′ have been reported.[25] However, LnOFs based on the ligand **L**′ have never been investigated in this field. In this work, we have synthesized a novel luminescent 2D lanthanide–organic framework, $\{[Tb_3(\mathbf{L})(\mu_3\text{-}OH)_7]\cdot H_2O\}_n$ (**1**) using ligand **L**′. **1** displays a rare 2D connectivity between Tb^{3+} ions and hydroxyl groups, and presents a distorted $CdCl_2$ type structure. To the best of our knowledge, it is extremely peculiar that the $CdCl_2$ type structure constructed with hydroxy groups and decorated with **L** was formed in the lanthanide N-heterocyclic coordination polymers. The luminescence intensity and lifetime as well as the thermal stability of **1**@PMMA were enhanced. Furthermore, the VT-luminescence properties and thermal stability of the polymer film materials have been investigated in detail.

Experimental section

Materials and instrumentation

All the reagents were commercially available and used without further purification. ^{1}H NMR (400 MHz) spectra were recorded on a Bruker ACF 400 MHz at room temperature. Infrared spectra were obtained from KBr pellets using a Nicolet Avatar-360 Infrared spectrometer in the 4000–400 cm^{-1} region. Elemental analyses were performed on a Perkin-Elmer 240c element analyzer. Inductively coupled plasma (ICP) analysis was performed on a Perkin-Elmer Model Optima 3300 DV ICP spectrometer. Powder X-ray diffraction (PXRD) patterns were recorded in the 2θ range of 5°–50° using Cu Kα radiation with a Shimadzu XRD-6000 X-ray diffractometer. UV-vis spectra were obtained on a Perkin-Elmer Lambda 20 spectrometer. The thermal analyses were performed on a ZRY-2P thermogravimetric analyzer from 30 °C to 700 °C with a heating rate of 10 °C min^{-1} under air. The simulation of XRPD pattern was carried out using the single-crystal data and diffraction-crystal module of the Mercury (Hg) program version 3.0.[26] All the fluorescence measurements were recorded on an Edinburgh FLS 920 luminescence spectrometer. The decay curves were fitted into a mono-exponential function: $I = I_0 + A\exp(-t/\tau)$, where I and I_0 are the luminescent intensities at time $t = t$ and $t = 0$, respectively, whereas τ is defined as the luminescent lifetime, and a double-exponential function: $I = I_0 + A_1\exp(-t/\tau_1) + A_2\exp(-t/\tau_2)$, where I and I_0 are the luminescent intensities at time $t = t$ and $t = 0$, respectively, whereas τ_1 and τ_2 are defined as the luminescent lifetimes. The average lifetime $<\tau>$ was calculated according to eqn (1):

$$<\tau> = \frac{\tau_1^2 A_1\% + \tau_2^2 A_2\%}{\tau_1 A_1\% + \tau_2 A_2\%}. \quad (1)$$

Synthesis of *N*,*N*′-bis(ethylacetate)biimidazole (L′). A solution containing 2,2′-biimidazole (0.01 mol), ethyl bromoacetate (0.02 mol) and NaOH (0.02 mol) in DMF (35 mL) was heated at 60 °C for 10 h. After wiping out the organic solvent, the mixture was precipitated with 200 mL of distilled water and then filtrated. The filtered solid was recrystallized from ethyl acetate to obtain a light-pink coloured product.[24] Yield: 43%. The ligand **L**′ was characterized by ^{1}H NMR, elemental analyses, UV-vis, and IR (Fig. S1†). Elemental Anal. Calcd for $C_{14}H_{18}N_4O_4$: C, 54.89; H, 5.92; N, 18.29. Found: C, 54.80; H, 5.90, N, 18.26. UV-vis (DMF): 284 nm. ^{1}H NMR (400 MHz, d_6-DMSO): δ = 1.17 (t, J = 8.0 Hz, 6H, $-CH_2CH_3$), δ = 4.13 (q, J = 4.0 Hz, 4H, $-CH_2CH_3$), δ = 5.37 (d, J = 6.0 Hz, 4H, $-CH_2-$), δ = 6.99 (d, J = 4.0 Hz, 2H, imidazole–H_3), δ = 7.26 (d, J = 8.0 Hz, 2H, imidazole–H_5). IR (KBr, cm^{-1}): 3464 (m), 3141 (w), 2993 (m), 1744 (s), 1519 (w), 1438 (m), 1377 (s), 1300 (m), 1233 (s), 1109 (m), 1026 (m), 881 (w), 753 (s), 690 (m), 580 (m).

Synthesis of $\{[Tb_3(L)(\mu_3\text{-}OH)_7]\cdot H_2O\}_n$ (1). A mixture of $Tb(NO_3)_3\cdot 6H_2O$ (0.1 mmol, 21.7 mg) and ligand **L**′ (0.15 mmol, 22.0 mg) with a molar ratio of 2 : 3 was mixed in H_2O (8 mL). After the mixture was stirred for 30 min in air, the pH of the reaction mixture was adjusted to 6.5 using sodium hydroxide and the resulting mixture was placed into a 20 mL Teflon-lined autoclave under autogenous pressure, heated at 165 °C for 72 h. After filtration, the products were washed with distilled water and then dried. Colorless crystals of **1** were obtained. Yield: 47% (based on terbium element). Elemental analysis (%) Calcd for **1**, $C_{10}H_{17}N_4O_{12}Tb_3$: C, 13.93; H, 1.99; N, 6.50. Found: C, 14.02, H, 1.96, N, 6.50. ICP analysis gave the following composition: Tb, 55.39% (calcd: 55.31%). IR (KBr pellet, cm^{-1}):

Table 1 Summary of crystallographic data for coordination polymer **1**

Data	**1**
Formula	$Tb_3C_{10}H_{17}N_4O_{12}$
Fw	862.04
Crystal system	Monoclinic
Space group	$P2_1/c$
a (Å)	13.187(3)
b (Å)	10.817(2)
c (Å)	12.567(3)
α (°)	90.00
β (°)	96.40(3)
γ (°)	90.00
V (Å^3)	1781.4(6)
Z	4
D_c (mg m^{-3})	3.214
μ (mm^{-1})	11.854
F (000)	1584
θ range for data collection (°)	3.03–27.48
Limiting indices	$-17 \le h \le 17$ $-14 \le k \le 13$ $-15 \le l \le 16$
Data/restraints/parameters	4071/0/262
Goodness of fit on F^2	1.063
Final R indices [$I > 2\sigma(I)$]	$R_1{}^a = 0.0324$, $wR_2{}^b = 0.0662$
R indices (all data)	$R_1{}^a = 0.0415$, $wR_2{}^b = 0.0696$
Largest diff. peak and hole (e Å^{-3})	1.855/−2.412

$^a R_1 = \sum||F_o| - |F_c||/\sum|F_o|$. $^b wR_2 = [\sum[w(F_o{}^2 - F_c{}^2)^2]/\sum[w(F_o{}^2)^2]]^{1/2}$.

3510 (br), 3139 (w), 3109 (w), 1597 (s), 1449 (s), 1394 (s), 1306 (m), 1127 (m), 916 (w), 753 (m), 679 (m), 583 (m).

Synthesis of PMMA doped with 1. PMMA was doped with coordination polymer **1** in proportions of 2.5%, 5.0%, 7.5%, 10.0% and 12.5%. The PMMA powder was dissolved in *N*,*N*′-dimethylformamide (DMF), followed by the addition of the required amount of **1** in DMF and the resulting mixture was heated at 50 °C for 60 min. The polymer film was obtained after evaporating the excess of solvent at 60 °C.

X-ray diffraction analysis

A suitable single crystal of **1** was carefully selected using an optical microscope and glued to thin glass fibers. The X-ray diffraction data for **1** was obtained at room temperature on a Siemens SMART 1000 CCD diffractometer equipped with graphite-monochromatic Mo Kα radiation (λ = 0.71073 Å). The crystal structure was resolved by a direct method and refined using a semi-empirical formula from equivalents and full-matrix least squares based on F^2 using the SHELXTL 5.1 software package.[27] All non-hydrogen atoms were anisotropically refined. Hydrogen atoms were fixed at calculated positions and refined using a riding mode, except for the water molecules. Table 1 shows the crystallographic crystal data and structure processing parameters used. Selected bond lengths and bond angles are listed in Table 2.

Results and discussion

In the synthetic process for ligand **L**′, the reaction mechanism is well-known N-alkylation reaction. Under neutral pH environment, which was obtained with the help of sodium hydroxide, ligand **L**′ underwent ester hydrolysis to produce ligand **L**. The reaction route is shown in Scheme 1.

In the IR spectra, the strong and broad band at 3200–3500 cm^{-1} indicates the presence of crystallization water molecules. A medium strong band at 2993 cm^{-1} was assigned to the –CH_2– vibrations. The strong absorption bands at around 1600 cm^{-1} and 1400 cm^{-1} were attributed to the asymmetric stretching vibrations (ν_{as}) and symmetric stretching vibrations (ν_s) of the carboxyl group, respectively. The absence of a strong band at 1744 cm^{-1} (Fig. S1†) for **1** indicates that the ligand **L**′ in **1** was hydrolyzed and deprotonated. PMMA was doped with coordination polymer **1** in proportions of 2.5%, 5.0%, 7.5%, 10.0%, and 12.5% (w/w), and characterized by IR spectroscopy, as shown in Fig. 1. The band at 1727 cm^{-1} for PMMA corresponds to the C=O vibration,[28] whereas for the **1**@PMMA polymer films, this vibration shifts to 1730 cm^{-1} and 1685 cm^{-1}. This implies that the Tb^{3+} coordination polymer was stabilized by means of interactions with the oxygen atoms of the carbonyl group in PMMA.[15,29] In the IR spectrum of **1**, the broad absorption band, which appears in the 3000–3500 cm^{-1} region was assigned to the O–H vibrational modes. Accordingly, the absence of the absorption band in the 3000–3500 cm^{-1} region confirmed that the doped PMMA polymer films were anhydrous. Therefore, the IR spectrum indicates that the carbonyl groups in PMMA replaced the water molecules in **1**@PMMA.

Single-crystal X-ray diffraction analysis of **1** reveals that it crystallizes in the monoclinic space group, $P2_1/c$, and the asymmetric unit consists of three crystallographically independent Tb^{3+} ions, one coordinated $\mathbf{L}^{2-}$ ligand, eleven μ_3-OH groups, and one free water molecule, as illustrated in Fig. 2. All the atoms localize on general positions. The metal center Tb1 is eight-coordinated by seven hydroxyl oxygen atoms (O5, O6, O8, O9, O10, O11, and O11A) and one carboxylic oxygen atom (O2) from ligand **L** in a distorted bi-capped trigonal prismatic geometry arrangement. Metal centers Tb2 and Tb3 are eight-coordinated by seven oxygen atoms coming from seven μ_3-OH groups and one carboxylic oxygen atom (Tb2 for O3, Tb3 for O1) to form a distorted bi-capped trigonal prismatic [TbO_8]. The ligand **L** displays a μ_3–η^1:η^1:η^1:η^0 coordination mode. The Tb1 atom is linked to two other terbium atoms (Tb3, Tb2) by μ_3-O11, μ_3-O6 (Tb1···Tb3 = 3.694 Å) and μ_3-O5, μ_3-O8, μ_3-O9 (Tb1···Tb2 = 3.915 Å) into a triangular [Tb_3O_{19}] unit. In addition, the two imidazole rings of **L** are almost coplanar with a deviation of about 5.981°. The Tb–O bond lengths fall in the range of 2.332(5)–2.530(4) Å. The O–Tb–O bond angles are in the range of 151.0(1)°–60.7(1)°. Among these, the O2–Tb1–O9, O6–Tb1–O8, O3–Tb2–O9 and O10A–Tb3–O11 bond angles are nearly vertical. All of the bond lengths and angles in **1** are within normal ranges and compatible with those for published terbium coordination polymers.[30]

In the structure of **1**, the Tb^{3+} ions are connected by hydroxyl groups giving rise to –M–O–M– infinite one-dimensional chains (Fig. 3a). Moreover, each Tb3 metal center is connected with three Tb1 and three Tb2 metal centers by hydroxyl

Table 2 Selected bond lengths (Å) and bond angles (°) for coordination polymer **1**[a]

Tb(1)–O(6)	2.361(4)	Tb(2)–O(3)	2.332(5)	Tb(3)–O(10)#6	2.334(4)
Tb(1)–O(5)	2.371(4)	Tb(2)–O(7)#4	2.351(5)	Tb(3)–O(1)	2.340(5)
Tb(1)–O(11)#1	2.378(4)	Tb(2)–O(7)	2.357(4)	Tb(3)–O(6)	2.386(4)
Tb(1)–O(2)	2.387(6)	Tb(2)–O(6)#5	2.363(4)	Tb(3)–O(9)#1	2.392(4)
Tb(1)–O(9)	2.402(4)	Tb(2)–O(10)#5	2.382(4)	Tb(3)–O(8)#6	2.400(4)
Tb(1)–O(8)	2.412(5)	Tb(2)–O(5)	2.423(4)	Tb(3)–O(5)#6	2.406(4)
Tb(1)–O(11)	2.470(4)	Tb(2)–O(8)	2.433(4)	Tb(3)–O(11)	2.440(4)
Tb(1)–O(10)	2.530(4)	Tb(2)–O(9)	2.442(4)	Tb(3)–O(7)#6	2.468(4)
Tb(1)–Tb(3)#2	3.6129(7)	Tb(2)–Tb(3)#2	3.5898(8)	Tb(3)–Tb(2)#6	3.5898(8)
Tb(1)–Tb(2)#3	3.9152(8)	Tb(2)–Tb(3)#5	3.8634(9)	Tb(3)–Tb(1)#6	3.6129(7)
Tb(1)–Tb(3)#1	3.9225(8)	Tb(2)–Tb(3)#1	3.8657(8)	Tb(3)–Tb(2)#6	3.8635(9)
Tb(1)–Tb(1)#1	3.9613(10)	Tb(2)–Tb(1)#5	3.9152(8)	Tb(3)–Tb(2)#3	3.8657(8)
O(6)–Tb(1)–O(5)	134.0(1)	O(3)–Tb(2)–O(7)#4	124.7(2)	O(10)#6–Tb(3)–O(1)	100.7(2)
O(6)–Tb(1)–O(11)#1	76.7(1)	O(3)–Tb(2)–O(7)	83.4(2)	O(10)#6–Tb(3)–O(6)	149.9(2)
O(5)–Tb(1)–O(11)#1	130.7(1)	O(7)#4–Tb(2)–O(7)	67.2(2)	O(1)–Tb(3)–O(6)	98.2(2)
O(6)–Tb(1)–O(2)	110.6(2)	O(3)–Tb(2)–O(6)#5	74.7(2)	O(10)#6–Tb(3)–O(9)#1	72.7(2)
O(5)–Tb(1)–O(2)	75.0(2)	O(7)#4–Tb(2)–O(6)#5	71.6(1)	O(1)–Tb(3)–O(9)#1	140.7(1)
O(11)#1–Tb(1)–O(2)	137.9(2)	O(7)–Tb(2)–O(6)#5	107.6(1)	O(6)–Tb(3)–O(9)#1	77.9(2)
O(6)–Tb(1)–O(9)	147.7(2)	O(3)–Tb(2)–O(10)#5	130.2(2)	O(10)#6–Tb(3)–O(8)#6	79.2(2)
O(5)–Tb(1)–O(9)	71.2(1)	O(7)#4–Tb(2)–O(10)#5	75.5(2)	O(1)–Tb(3)–O(8)#6	136.7(2)
O(11)#1–Tb(1)–O(9)	71.0(2)	O(7)–Tb(2)–O(10)#5	140.6(2)	O(6)–Tb(3)–O(8)#6	102.3(2)
O(2)–Tb(1)–O(9)	94.0(2)	O(6)#5–Tb(2)–O(10)#5	70.6(1)	O(9)#1–Tb(3)–O(8)#6	81.3(1)
O(6)–Tb(1)–O(8)	94.4(2)	O(3)–Tb(2)–O(5)	75.9(2)	O(10)#6–Tb(3)–O(5)#6	70.8(1)
O(5)–Tb(1)–O(8)	61.7(1)	O(7)#4–Tb(2)–O(5)	128.3(1)	O(1)–Tb(3)–O(5)#6	77.6(2)
O(11)#1–Tb(1)–O(8)	82.1(1)	O(7)–Tb(2)–O(5)	69.8(1)	O(6)–Tb(3)–O(5)#6	136.7(1)
O(2)–Tb(1)–O(8)	135.7(2)	O(6)#5–Tb(2)–O(5)	150.6(2)	O(9)#1–Tb(3)–O(5)#6	131.3(1)
O(9)–Tb(1)–O(8)	80.8(2)	O(10)#5–Tb(2)–O(5)	130.8(1)	O(8)#6–Tb(3)–O(5)#6	61.3(2)
O(6)–Tb(1)–O(11)	71.1(1)	O(3)–Tb(2)–O(8)	136.5(2)	O(10)#6–Tb(3)–O(11)	92.9(2)
O(5)–Tb(1)–O(11)	145.5(2)	O(7)#4–Tb(2)–O(8)	84.7(2)	O(1)–Tb(3)–O(11)	71.6(1)
O(11)#1–Tb(1)–O(11)	70.4(2)	O(7)–Tb(2)–O(8)	80.2(1)	O(6)–Tb(3)–O(11)	71.2(2)
O(2)–Tb(1)–O(11)	73.2(2)	O(6)#5–Tb(2)–O(8)	148.8(2)	O(9)#1–Tb(3)–O(11)	70.1(2)
O(9)–Tb(1)–O(11)	98.1(1)	O(10)#5–Tb(2)–O(8)	84.2(1)	O(8)#6–Tb(3)–O(11)	151.4(1)
O(8)–Tb(1)–O(11)	151.0(2)	O(5)–Tb(2)–O(8)	60.7(1)	O(5)#6–Tb(3)–O(11)	141.7(2)
O(6)–Tb(1)–O(10)	68.1(1)	O(3)–Tb(2)–O(9)	87.6(2)	O(10)#6–Tb(3)–O(7)#6	138.9(1)
O(5)–Tb(1)–O(10)	68.0(1)	O(7)#4–Tb(2)–O(9)	144.1(2)	O(1)–Tb(3)–O(7)#6	73.7(2)
O(11)#1–Tb(1)–O(10)	135.9(2)	O(7)–Tb(2)–O(9)	139.5(1)	O(6)–Tb(3)–O(7)#6	69.2(1)
O(2)–Tb(1)–O(10)	80.9(2)	O(6)#5–Tb(2)–O(9)	107.9(1)	O(9)#1–Tb(3)–O(7)#6	136.3(2)
O(9)–Tb(1)–O(10)	138.8(2)	O(10)#5–Tb(2)–O(9)	70.9(2)	O(8)#6–Tb(3)–O(7)#6	78.7(1)
O(8)–Tb(1)–O(10)	75.3(1)	O(5)–Tb(2)–O(9)	69.7(1)	O(5)#6–Tb(3)–O(7)#6	68.3(1)
O(11)–Tb(1)–O(10)	118.9(1)	O(8)–Tb(2)–O(9)	79.6(1)	O(11)–Tb(3)–O(7)#6	121.7(1)

[a] Symmetry transformations used to generate equivalent atoms: #1: $-x+1, -y, -z+1$; #2: $x, -y+1/2, z+1/2$; #3: $-x+1, y+1/2, -z+3/2$; #4: $-x+1, -y, -z+2$; #5: $-x+1, y-1/2, -z+3/2$; #6: $x, -y+1/2, z-1/2$.

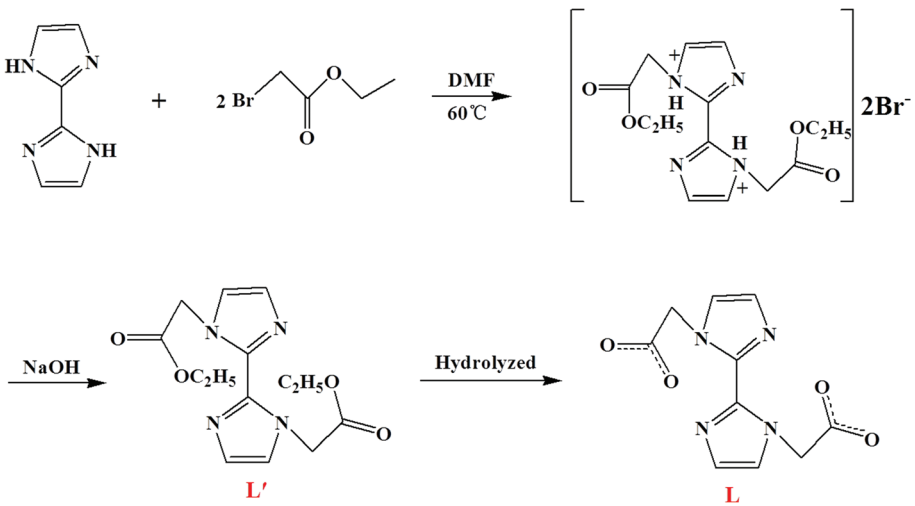

Scheme 1 Synthetic procedure for ligands L′ and L.

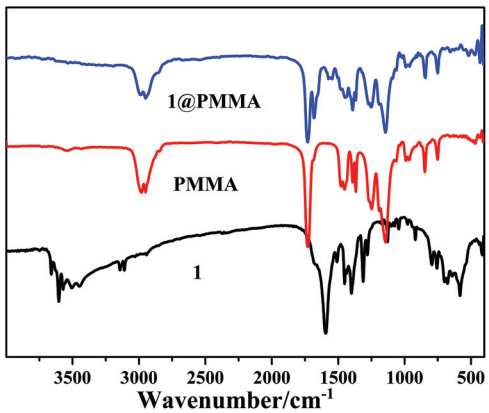

Fig. 1 IR spectra of **1**, pure PMMA, and **1**@PMMA polymer film.

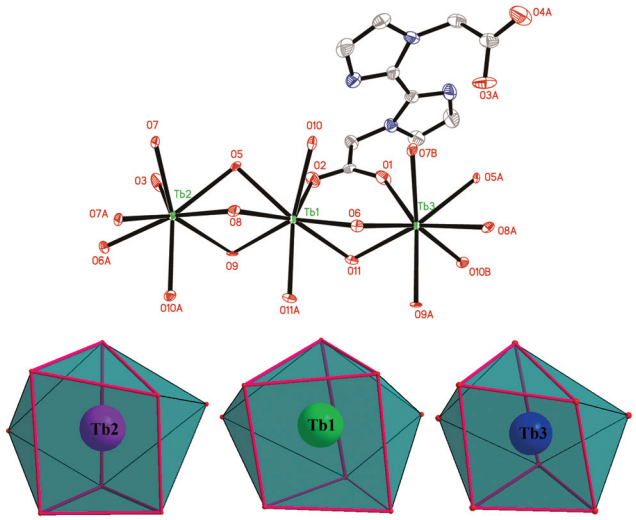

Fig. 2 The coordination environment of Tb^{3+} ion in the coordination polymer **1** with 50% thermal ellipsoids (hydrogen atoms on the carbon atoms have been omitted for clarity. (A) 1 − *x*, *y*, 1 − *z*; (B) *x*, 0.5 − *y*, −0.5 + *z*) and the corresponding coordination polyhedron of Tb^{3+} ions in coordination polymer **1** (Tb1 for green spheres; Tb2 for pink spheres, and Tb3 for blue spheres).

groups in different directions, resulting in a six-membered ring. Moreover, every Tb1 and Tb2 is also connected with the surrounding six metal centres *via* hydroxyl groups, extending into a 2D layer structure along the *bc* plane, as shown in Fig. 3b. Coordination polymer **1** displays two-dimensional connectivity between the Tb^{3+} ions and hydroxyl groups with a distorted $CdCl_2$ type structure. This is the first observation of a $CdCl_2$ type structure constructed by hydroxy groups and decorated with ligand **L**, to the best of our knowledge, in lanthanide N-heterocyclic coordination polymers. According to the Lewis acid–base concept and Pearson's hard–soft acid–base principle, rare earth cations are hard acids.[31] They are easy to coordinate with hard base atoms such as F, O and N atoms. Compared with N atoms, rare earth cations are liable to coordinate with O atoms. Thus, in coordination polymer **1**, Tb^{3+} ions only coordinate with O atoms, while N atoms from ligand **L** are uncoordinated.

The results of the powder X-ray diffraction (PXRD) measurements indicates that the peaks displayed in the measured PXRD patterns closely match to those in the simulated patterns that were generated from the single-crystal diffraction data, demonstrating the phase purity of **1** (Fig. S2†). The differences in intensities may be attributed to the preferred orientation of the powder samples.[32]

The UV-vis absorption spectra of ligand **L′** and **1** were measured in DMF solution at room temperature ($c = 1 \times 10^{-5}$ M). As illustrated in Fig. 4, the maximum absorption bands were at 284 nm for ligand **L′** and 296 nm for **1**. The ligand **L′** reveals an absorption band in its UV spectrum, which corresponds to the singlet–singlet π–π* transition from the imidazole-based moiety.[33] The absorption spectrum of **1** is similar to that of the free ligand, which indicates that the singlet excited state of the ligand is not under the influence of metal coordination. Because of the low extinction coefficients of the Laporte forbidden f–f transitions, lanthanide ions present weak absorption of ultraviolet radiation. In addition, a small red shift in the absorption spectrum of **1** was caused by the metal perturbed intra-ligand π–π* transition.[34] The molar absorption coefficient value of 7968 L mol^{-1} cm^{-1} for **1** is higher than 3973 L mol^{-1} cm^{-1} for the ligand **L′**. Moreover, the large molar absorption coefficient of ligand **L′** implies that it has a strong ability to absorb light.[35]

The visible luminescence spectra of **1** were recorded in the solid state and in DMF solution at ambient temperature. The excitation spectra were monitored around the more intense emission line at 544 nm for Tb^{3+} ions. As shown in Fig. S3,† the excitation spectra of **1** displays a large broad band. It is the same as the structured profile for the UV spectral region (290–310 nm) that can be assigned to the electronic transition of ligand. The absence of any absorption bands due to the f–f transitions of Tb^{3+} ions proves that luminescence sensitization *via* ligand excitation is effective.[9,36] The emission spectrum of **1** shows characteristic Tb^{3+} metal-centered and ligand-centered (401 nm) luminescence. The ligand-centered emission was blue-shifted by 11 nm compared with the free ligand (412 nm, Fig. S4†), which may be attributed to the metal disturbed ligand-centered π*→π transitions. The ambient-temperature emission spectrum of **1** shows characteristics of a Tb^{3+}-centered $^5D_4$ excited to the ^7F_J ground state multiplet. Maximum peak intensities at 489, 544, 586, 620, and 649 nm were observed for J = 6, 5, 4, 3, and 2 transitions, respectively.[37,38] The most intense emission at 544 nm corresponds to the $^5D_4 \rightarrow {}^7F_5$ hypersensitive transition of Tb^{3+} ion. However, the transitions to ^7F_J (J = 1, 0) levels were too weak to measure. It is noteworthy that the emission peak positions do not change in solvent. As illustrated in Fig. 5, the most intense emission at 544 nm and second intense emission at 489 nm of Tb^{3+} ion are almost the same. The remaining three transitions of Tb^{3+} ion are slightly stronger in the solid state than that found in the DMF solution. The ligand-centered (401 nm) luminescence intensity in DMF solution was nearly twice higher than that

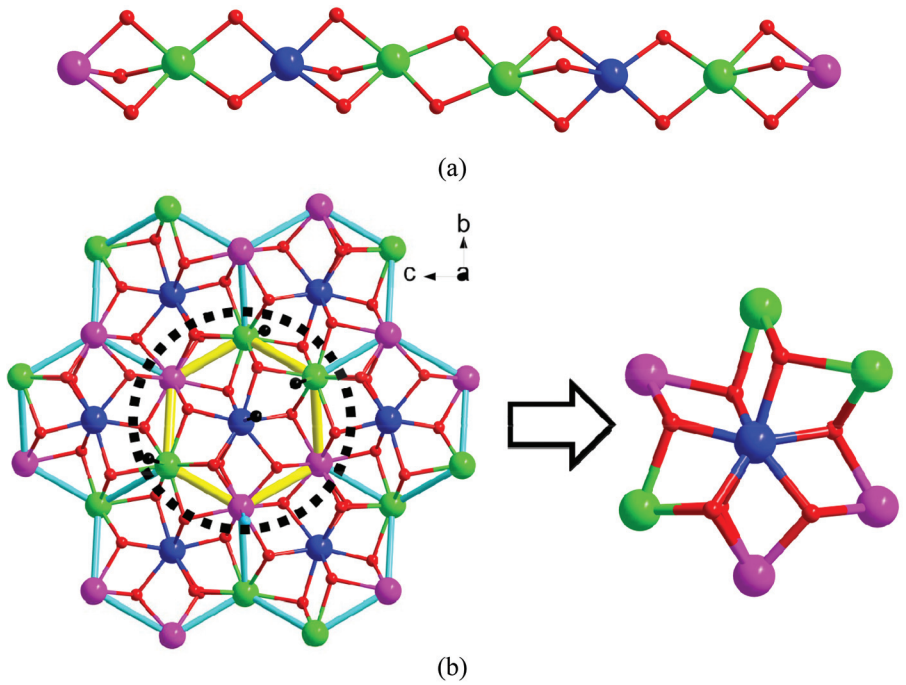

Fig. 3 (a) The one-dimensional chains of coordination polymer **1**; (b) connectivity between the six connected Tb^{3+} ions and the three connected hydroxyl groups moieties (red spheres) forming a $CdCl_2$ type two-dimensional structure.

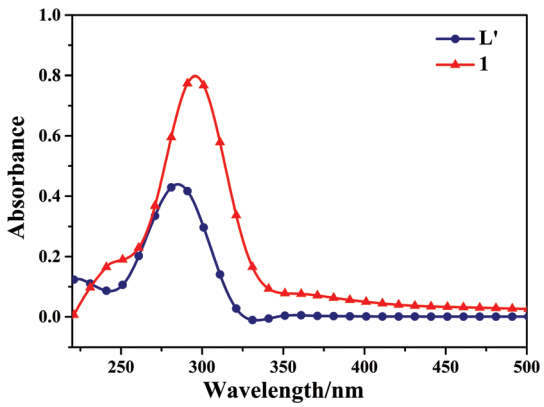

Fig. 4 UV-vis absorption spectra of ligand L' and **1** in DMF solution (c = 1×10^{-5} M).

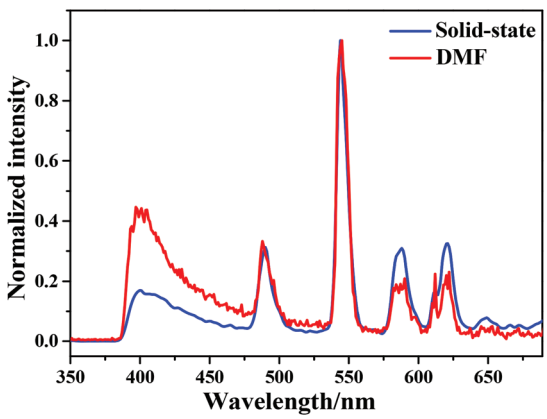

Fig. 5 The normalized emission spectra of coordination polymer **1** in the solid-state and DMF solution at 298 K.

found in the solid state. Therefore, coordination polymer **1** emits green luminescence under different conditions. All the luminescence data are listed in Table 3.

The fluorescence lifetimes of **1** were measured on an Edinburgh Instruments FLS 920 spectrometer monitored around the strongest emission ($^5D_4 \rightarrow {}^7F_5$) for Tb^{3+} ions. As shown in Fig. S5,† the typical decay profiles for **1** in the solid state reveal double exponential functions at 298 K, indicating the presence of more than one emissive Tb^{3+} ion center.[29] The considerably shorter lifetime for **1** compared with the Tb-carboxylate coordination polymers previously reported[39] was attributed to the vibronic coupling induced by the presence of solvent molecules and hydroxyl groups in the crystal structure.[40] The luminescence lifetimes of **1** are τ_1 = 76.45 μs (53.89%) and τ_2 = 240.71 μs (46.11%) in the solid-state, which were well fitted to the double-exponential function,[41] and τ = 1258.8 μs (100%) in DMF solution, which was well fitted to the mono-

Table 3 Luminescence data for coordination polymer **1** and **1**@PMMA

	Excitation [nm]	Emission [nm]	Integrated area	Lifetime [μs]
1-solid sate	300	544	23 593	196.24
1-DMF solution	300	544	35 653	1258.8
1@2.5%PMMA	300	544	26 139	818.35
1@5%PMMA	300	544	32 495	893.35
1@7.5%PMMA	300	544	58 747	904.64
1@10%PMMA	300	544	120 537	914.88
1@12.5%PMMA	300	544	28 152	901.11

exponential function.[42] The correlation coefficients were 1.201 and 1.321, respectively. According to the model reported in the literature,[43,44] the existence of the strong Tb–Tb interaction in the solid state, which increases the collisional quenching of the excited-state molecular, results in a decrease of the luminescence lifetime.

Lanthanide coordination polymers incorporated into polymer matrixes represent a new class of materials. The materials possess the characteristics of both complexes and polymers, and can serve as ideal candidates in a wide range of new technologies.[16,45] As an extension of this work, we described the incorporation of the newly designed and intensely luminescent **1** into PMMA, a well-known, low-cost, and easily prepared polymer with excellent optical quality. The excitation spectra of the PMMA polymer films doped with $\{[Tb_3(\mathbf{L})(\mu_3\text{-}OH)_7]\cdot H_2O\}_n$ at different concentrations [2.5, 5.0, 7.5, 10.0, and 12.5% (w/w)] are shown in Fig. S6.† The emission spectra of PMMA doped with coordination polymer **1** at a variety of concentrations (λ_{ex} = 300 nm) exhibit five emission bands that are assigned to the characteristic $^5D_4 \rightarrow {}^7F_J$ (J = 6–2) transitions of the Tb^{3+} ion. When analyzed by plotting (Fig. S7†), the luminescence intensity was like a parabola, which is affected by the concentration of **1**. Moreover, the luminescence intensity of the Tb^{3+} excitation and emission bands increased with the concentration of **1** from 2.5% to 10%. The emission intensity reaches the maximum at a concentration of 10%, as shown in Fig. 7. When the concentration was higher than the maximum value, the luminescence intensity decreased. As the coordination polymer content increased from 10% to 12.5% in the PMMA matrix, the O–H substitution ability of PMMA was gradually decreased. It is exactly the stretching vibration of O–H, which caused the luminescence quenching. The luminescent emission spectra reveals that the intensity of the thin film was essentially increased in contrast to that found for **1**, which indicates that PMMA plays a vital role in the luminescent features of the polymer film materials. The results were also proved by the integrated area of the $^5D_4 \rightarrow {}^7F_5$ transitions. The maximum integrated area reached to 35 653 at a Tb^{3+} content of 10%. The PMMA enhances the light absorption of cross-section so that more energy can be transferred to the central Tb^{3+} ions (Fig. 6).

The emission decays were analyzed by the sum of the exponential functions. The typical luminescence decay curves for the excited Tb^{3+} ions in the $^5D_4$ state under excitation at 300 nm are illustrated in Fig. 7, which can be described as a double-exponential function within experimental errors. Notably, with an increase in the content of **1**, the lifetimes of **1**@PMMA films increased and reached the maximum at 10% (τ = 914.88 μs), which is more than four times longer than that found for **1** (τ = 196.24 μs), and then decreased upon a further increase of the content of coordination polymer **1**. All the τ values for the doped polymer systems are higher than that found for the coordination polymer **1**. This indicates that radiative processes are operative in all the doped polymer films because of the absence of multiphonon relaxation by coupling with the O–H oscillators from $\{[Tb_3(\mathbf{L})(\mu_3\text{-}OH)_7]\cdot H_2O\}_n$.[46]

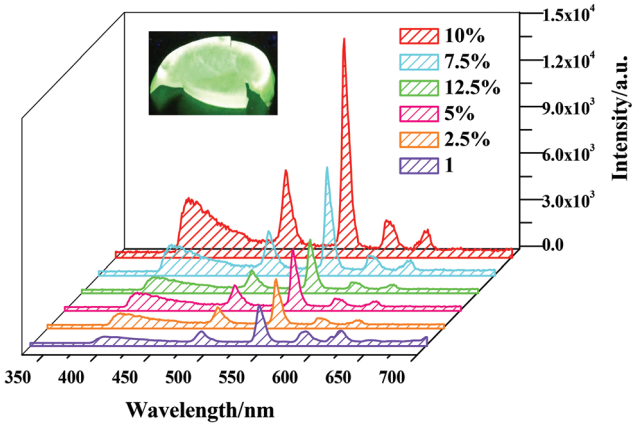

Fig. 6 The emission spectra of coordination polymer **1** and PMMA polymer doped with coordination polymer **1** (2.5%–12.5%) at 298 K under excitation at 300 nm.

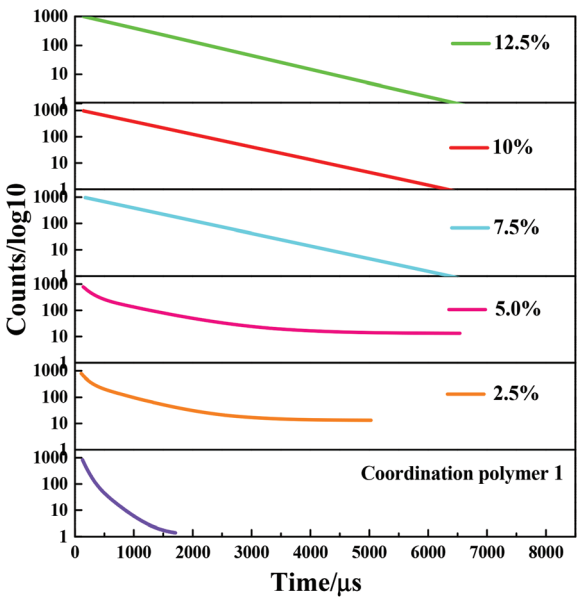

Fig. 7 Luminescence decay curves monitoring the excitation at 300 nm and emission at 544 nm of the PMMA polymer doped with coordination polymer **1** in the concentration range of 2.5%–12.5%.

The variable-temperature luminescence properties of **1**@PMMA were investigated in the solid-state because of the good luminescent properties of **1**@PMMA. Coordination polymer **1** maintains its luminescence up to at least 270 °C, which is close to its decomposition temperature of 280 °C.[47] The emission spectra in the solid-state at different temperature (303 K–543 K, step: 20 K) are displayed in Fig. 8. Upon excitation at 302 nm, **1**@PMMA exhibits five emission bands that are assigned to the characteristic $^5D_4 \rightarrow {}^7F_J$ (J = 6–2) transitions of the Tb^{3+} ion. The most interesting phenomenon in the emission spectra of **1**@PMMA at different temperatures is that the intensities of the main bands are almost unchanged. Thus, temperatures below 343 K do not change the fluorescence properties of **1**@PMMA and it has a stable green

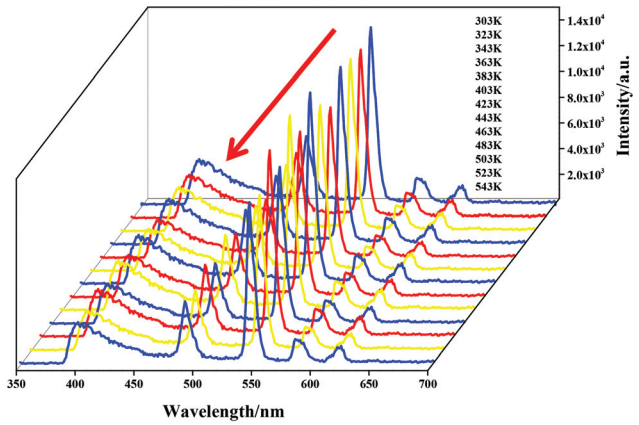

Fig. 8 Emission spectra of PMMA polymer doped with 10% coordination polymer **1** at different temperatures (303 K–543 K, step: 20 K) under excitation at 302 nm.

fluorescence performance at different temperatures. **1**@PMMA could be used as a new type of organic fluorescent glass with optical transfer function. This new type of organic fluorescent glass has characteristics of strong plasticity, resistance to chemical corrosion and good hardness like organic glass. Therefore, it can be widely used in colored doors and windows, mobile phone lenses, and plastic optical fiber.

For the determination of the thermal properties of **1** and **1**@PMMA, exemplary simultaneous TG/DTA investigations were carried out and the results are reported in Fig. 9. The TGA curve for coordination polymer **1** displays a first weight loss of 4.9% up to 250 °C, which corresponds to the loss of coordinated water (calcd 2.1%) and undried water molecules. The second weight loss of 28.7% (calcd 29.9%) from 330 to 560 °C with an exothermic DTA peak at 425 °C corresponds to the decomposition of L^{2-} ligands. The remaining product could be Tb_2O_3, which is in good agreement with the experimental results (obs 66.2%, calcd 68.0%).[48,49] The TG analysis of PMMA and **1**@PMMA hybrid materials exhibit no weight-loss in the temperature region of 50–250 °C in contrast to that found for the coordination polymer **1**. This demonstrates that the water molecules or hydroxyl groups in coordination polymer **1** may be replaced by carbonyl groups after doping into PMMA. Such a conclusion is in good agreement with the IR analyses of the doped hybrid materials.[23] The major weight loss occurs from 280 to 400 °C, which suggests that the thermal stability of the **1**@PMMA polymer film was improved upon doping with coordination polymer **1**.

Conclusions

In conclusion, the newly synthesized Tb coordination polymer based on *N*,*N*′-bis(ethylacetate)biimidazole (**L**′) have a significant effect on the performance of polymer film materials when it was doped into PMMA matrix; it could improve both the luminescence intensity and luminescence lifetime. ligand **L**′ was synthesized by an N-alkylation reaction process and ester hydrolysis was used to produce ligand **L**. Coordination polymer **1** is a rare 2D net with distorted $CdCl_2$ type structure, which is connected by Tb^{3+} ions and hydroxyl groups. This work was extended by doping coordination polymer **1** into a PMMA matrix to obtain a PMMA-supported doped polymer film materials, which display excellent green luminescent properties with enhanced luminescence intensity, long lifetimes and thermal stability. The PMMA matrix acts as a co-sensitizer for Tb^{3+} ions. Moreover, the VT-luminescence investigations confirm that **1**@PMMA can be used as a type of stable green luminescence material below 343 K. These results intend to be a contribution to the development of LnOFs based on imidazole-carboxylate ligands, which can be used in the pursuit of applications in farm plastic-film with optical transfer function.

Acknowledgements

This work was supported by the National Natural Science Foundation of China (grant 21371040 and 21171044), the National key Basic Research Program of China (973 Program, no. 2013CB632900), Fundamental Research Funds for the Central Universities (grant no. HIT. IBRSEM. A. 201409), and the Program for Innovation Research of Science in Harbin

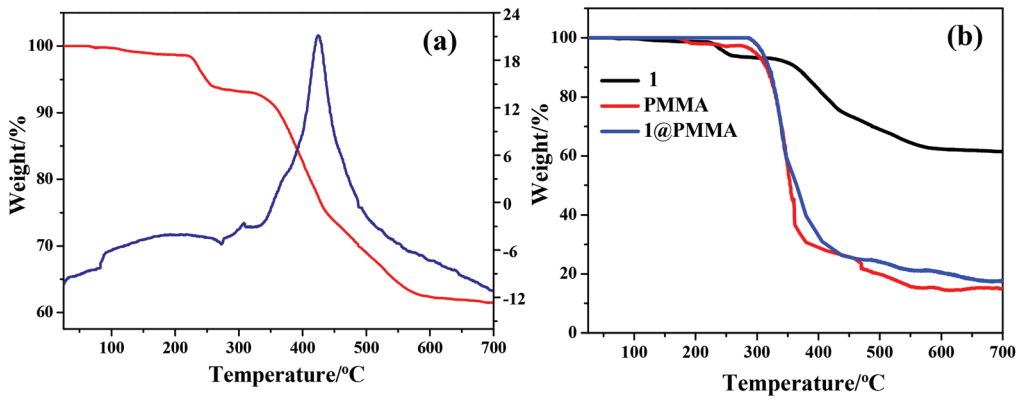

Fig. 9 (a) The TG/DTA curves of **1**. (b) The comparison of TG curves of pure PMMA, **1**, and **1**@PMMA.

Institute of Technology (PIRS of HIT no. A201416 and B201414).

References

1 X. J. Zhang, M. A. Ballem, M. Ahrén, A. Suska, P. Bergman and K. Uvdal, *J. Am. Chem. Soc.*, 2010, **132**, 10391.
2 J. Wu, Z. Q. Ye, G. L. Wang, D. Y. Jin, J. L. Yuan, Y. F. Guan and J. Piper, *J. Mater. Chem.*, 2009, **19**, 1258.
3 P. Mahata, K. V. Ramya and S. Natarajan, *Chem. – Eur. J.*, 2008, **14**, 5839.
4 C. J. Gao, A. M. Kirillov, W. Dou, X. L. Tang, L. L. Liu, X. H. Yan, Y. J. Xie, P. X. Zang, W. S. Liu and Y. Tang, *Inorg. Chem.*, 2014, **53**, 935.
5 Z. Q. Jiang, G. Y. Jiang, D. C. Hou, F. Wang, Z. Zhao and J. Zhang, *CrystEngComm*, 2013, **15**, 315.
6 D. B. A. Raj, S. Biju and M. L. P. Reddy, *J. Mater. Chem.*, 2009, **19**, 7976–7983.
7 Y. J. Cui, Y. F. Yue, G. D. Qian and B. L. Chen, *Chem. Rev.*, 2012, **112**, 1126–1162.
8 M. O. Rodrigues, N. B. D. Júnior, C. A. D. Simone, A. A. S. Araújo, A. M. Brito-Silva, F. A. A. Paz, M. E. D. Mesquita, S. A. Júnior and R. O. Freire, *J. Phys. Chem. B*, 2008, **112**, 4204.
9 M. L. P. Reddy, V. Divya and R. Pavithran, *Dalton Trans.*, 2013, **42**, 15249.
10 Y. Q. Sun, J. Zhang and G. Y. Yang, *Chem. Commun.*, 2006, 4700.
11 Y. H. Xu, Y. Q. Lan, X. L. Wang, H. Y. Zang, K. Z. Shao, Y. Liao and Z. M. Su, *Solid State Sci.*, 2009, **11**, 635.
12 R. Haldar and T. K. Maji, *CrystEngComm*, 2013, **15**, 9276.
13 M. H. Alkordi, J. A. Brant, L. Wojtas, V. C. Kravtsov, A. J. Cairns and M. Eddaoudi, *J. Am. Chem. Soc.*, 2009, **131**, 17753.
14 Y. H. Zhang, X. Li and S. Song, *Chem. Commun.*, 2013, **49**, 10397.
15 D. B. A. Raj, B. J. Francis, M. L. P. Reddy, R. R. Butorac, V. M. Lynch and A. H. Cowley, *Inorg. Chem.*, 2010, **49**, 9055.
16 J. Kai, M. C. F. C. Felinto, L. A. O. Nunes, O. L. Malta and H. F. Brito, *J. Mater. Chem.*, 2011, **21**, 3796.
17 H. F. Li, P. F. Yan, P. Chen, Y. Wang, H. Xu and G. M. Li, *Dalton Trans.*, 2012, **41**, 900.
18 X. Zhao, B. Xiao, A. J. Fletcher, K. M. Thomas, D. Bradshaw and M. J. Rosseinsky, *Science*, 2004, **306**, 1012.
19 S. I. Klink, L. Grave, D. N. Reinhoudt, F. C. J. M. van Veggel, M. H. V. Werts, F. A. J. Geurts and J. W. Hofstraat, *J. Phys. Chem. A*, 2000, **104**, 5457.
20 Y. Hasegawa, M. Yamamuro, Y. J. Wada, N. Kanehisa, Y. Kai and S. Yanagida, *J. Phys. Chem. A*, 2003, **107**, 1697.
21 W. Q. Fan, J. Feng, S. Y. Song, Y. Q. Lei, G. L. Zheng and H. J. Zhang, *Chem. – Eur. J.*, 2010, **16**, 1903.
22 H. X. Huang, J. Liu and Y. Q. Cai, *J. Lumin.*, 2013, **143**, 447.
23 W. Z. Li, P. F. Yan, G. F. Hou, H. F. Li and G. M. Li, *Dalton Trans.*, 2013, **42**, 11537.
24 K. Miyata, Y. Konno, T. Nakanishi, A. Kobayashi, M. Kato, K. Fushimi and Y. Hasegawa, *Angew. Chem., Int. Ed.*, 2013, **52**, 6413.
25 Y. H. Xu, Y. Q. Lan, S. X. Wu, K. Z. Shao, Z. M. Su and Y. Liao, *CrystEngComm*, 2009, **11**, 1711.
26 C. F. Macrae, P. R. Edgington, P. McCabe, E. Pidcock, G. P. Shields, P. Taylor, M. Towler and J. van de Streek, *J. Appl. Crystallogr.*, 2006, **39**, 453.
27 N. T. Shelxtl, *Crystal structure analysis package, version 5.10*, Bruker AXS, Analytical X-ray System, Madison, WI, 1999.
28 H. G. Liu, Y. I. Lee, W. P. Qin, K. W. K. Jang, S. Kim and X. S. Feng, *J. Appl. Polym. Sci.*, 2004, **92**, 3524.
29 W. Z. Li, P. F. Yan, G. F. Hou, H. F. Li and G. M. Li, *RSC Adv.*, 2013, **3**, 18173.
30 H. B. Zhang, L. J. Zhou, J. Wei, Z. H. Li, P. Lin and S. W. Du, *J. Mater. Chem.*, 2012, **22**, 21210.
31 Q. Y. Liu, W. F. Wang, Y. L. Wang, Z. M. Shan, M. S. Wang and J. K. Tang, *Inorg. Chem.*, 2012, **51**, 2381.
32 C. J. Höller, P. R. Matthes, M. Adlung, C. Wickleder and K. Müller-Buschbaum, *Eur. J. Inorg. Chem.*, 2012, **33**, 5479.
33 H. H. Hammud, A. Ghannoum and M. S. Masoud, *Spectrochim. Acta, Part A*, 2006, **63**, 255.
34 W. T. Xu, Y. F. Zhou, D. C. Huang, W. Xiong, M. Y. Su, K. Wang, S. Han and M. C. Hong, *Cryst. Growth Des.*, 2013, **13**, 5420.
35 E. G. Moore, A. P. S. Samuel and K. N. Raymond, *Acc. Chem. Res.*, 2009, **42**, 542.
36 A. P. S. Samuel, E. G. Moore, M. Melchior, J. D. Xu and K. N. Raymond, *Inorg. Chem.*, 2008, **47**, 7537.
37 J. D. Xu, T. M. Corneillie, E. G. Moore, G. L. Law, N. G. Butlin and K. N. Raymond, *J. Am. Chem. Soc.*, 2011, **133**, 19900.
38 C. B. Liu, Q. Li, X. Wang, G. B. Che and X. J. Zhang, *Inorg. Chem. Commun.*, 2014, **39**, 56.
39 P. R. Matthes, J. Nitsh, A. Kuzmanoski, C. Feldmann, A. Steffen, T. B. Marder and K. Müller-Buschbaum, *Chem. – Eur. J.*, 2013, **19**, 17369.
40 P. Wang, R. Q. Fan, X. R. Liu, L. Y. Wang, Y. L. Yang, W. W. Cao, B. Yang, W. L. J. Hasi, Q. Su and Y. Mu, *CrystEngComm*, 2013, **15**, 1931.
41 E. G. Moore, G. Szigethy, J. D. Xu, L. O. Pålsson, A. Beeby and K. N. Raymond, *Angew. Chem., Int. Ed.*, 2008, **47**, 9500.
42 A. Rodríguez-Diéguez, A. Salinas-Castillo, A. Sironi, J. M. Seco and E. Colacio, *CrystEngComm*, 2010, **12**, 1876.
43 M. Yokota and O. Tanimoto, *J. Phys. Soc. Jpn.*, 1967, **22**, 779.
44 M. Inokuti and F. Hirayama, *J. Chem. Phys.*, 1965, **43**, 1978.
45 H. G. Liu, Y. I. Lee, S. Park, K. Jang and S. S. Kim, *J. Lumin.*, 2004, **110**, 11–16.
46 H. X. Huang, J. Liu and Y. Q. Cai, *J. Lumin.*, 2013, **143**, 447.
47 N. B. Shustova, A. F. Cozzolino, S. Reineke, M. Baldo and M. Dincă, *J. Am. Chem. Soc.*, 2013, **135**, 13326.
48 X. Lim, X. H. Zhao, Y. Bing, M. Q. Zhao, H. Z. Xie and Z. Y. Guo, *J. Solid State Chem.*, 2013, **197**, 81.
49 D. T. de Lill and C. L. Cahill, *Chem. Commun.*, 2006, 4946.